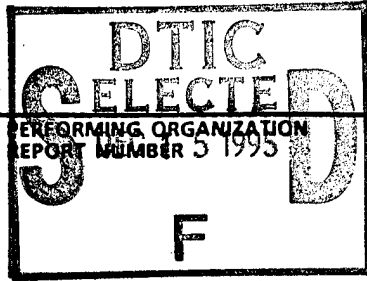


REPORT DOCUMENTATION PAGE

Form Approved
OMB No. 0704-0188

Public reporting burden for this collection of information is estimated to average 1 hour per response, including the time for reviewing instructions, searching existing data sources, gathering and maintaining the data needed, and completing and reviewing the collection of information. Send comments regarding this burden estimate or any other aspect of this collection of information, including suggestions for reducing this burden, to Washington Headquarters Services, Directorate for Information Operations and Reports, 1215 Jefferson Davis Highway, Suite 1204, Arlington, VA 22202-4302, and to the Office of Management and Budget, Paperwork Reduction Project (0704-0188), Washington, DC 20503.

1. AGENCY USE ONLY (Leave blank)		2. REPORT DATE September 12, 1995	3. REPORT TYPE AND DATES COVERED Final Technical Report	
4. TITLE AND SUBTITLE Novel, Programmable Broadband Fiber-Optic Delay Line Networks			5. FUNDING NUMBERS DAAL01-95-C-2017	
6. AUTHOR(S) James H. Bechtel				
7. PERFORMING ORGANIZATION NAME(S) AND ADDRESS(ES) TACAN Corporation 2330 Faraday Avenue Carlsbad, CA 92008				
9. SPONSORING/MONITORING AGENCY NAME(S) AND ADDRESS(ES) Department of the Army U.S. Army Research Laboratory White Sands Missile Range NM 88002-5513			8. PERFORMING ORGANIZATION REPORT NUMBER 3 1995	
10. SPONSORING/MONITORING AGENCY REPORT NUMBER				
11. SUPPLEMENTARY NOTES <div style="border: 1px solid black; padding: 5px; text-align: center;"> DISTRIBUTION STATEMENT A Approved for public release Distribution Unlimited </div>				
12a. DISTRIBUTION/AVAILABILITY STATEMENT Views, opinions, and/or findings contained in this report are those of the author(s) and should not be construed as an official Department of the Army position, policy, or discussion unless so designated by other documentation.			12b. DISTRIBUTION CODE	
13. ABSTRACT (Maximum 200 words) The objective of this Phase I work is to develop new designs and approaches to digitally-programmable, fiber-optic delay lines for wideband microwave signals. Our unique approach will use novel, polymeric switches and electro-optical modulators together with a 1550 nm source and optical fiber amplifiers and fiber delay lines. The use of polymer switches and modulators provides not only very large bandwidth modulation but also fast switching time with low insertion loss and high isolation. The nonlinear optical polymers provide devices with large electro-optic coefficients, small dispersion, larger frequency response (potentially to 100 GHz), fast switching speed, and greater fabrication flexibility compared to LiNbO ₃ or GaAs waveguide technology. Various types of polymer-based modulators and switches with optical fiber amplifiers were considered in Phase I for applications to programmable fiber-optic delay line networks and device development in Phase II. Military applications include radar simulation and other microwave and millimeter wave uses. The development of these devices will eventually lead to the use of modulators and switches in photonic integrated circuits. Modulator applications include single or multichannel RF distribution, cable TV distribution, analog sensor data links, radar signal distribution, and other fiber-optic systems.				
14. SUBJECT TERMS 19951213 021			15. NUMBER OF PAGES 27	
			16. PRICE CODE	
17. SECURITY CLASSIFICATION OF REPORT UNCLASSIFIED	18. SECURITY CLASSIFICATION OF THIS PAGE UNCLASSIFIED	19. SECURITY CLASSIFICATION OF ABSTRACT UNCLASSIFIED	20. LIMITATION OF ABSTRACT UNCLASSIFIED	

Novel, Programmable Broadband Fiber-Optic Delay Line Networks

Final Technical Report

Contract #DAAL01-95-C-2017

DEPARTMENT OF THE ARMY
U.S. Army Research Laboratory
White Sands Missile Range NM 88002-5513

Submitted by

TACAN Corporation
2330 Faraday Avenue
Carlsbad, California 92008
(619) 438-1010

Unclassified

Views, opinions, and/or findings contained in this report are those of the author(s) and should not be construed as an official Department of the Army position, policy, or decision unless so designated by other documentation.

TABLE OF CONTENTS

	Page
ABSTRACT	2
TABLE OF CONTENTS	3
I. INTRODUCTION	4
II. PHASE I RESULTS	8
III. CONCLUSIONS	27
IV. FUTURE WORK	27

Accession For	
NTIS CRA&I	<input checked="" type="checkbox"/>
DTIC TAB	<input type="checkbox"/>
Unannounced	<input type="checkbox"/>
Justification	
By	
Distribution /	
Availability Codes	
Dist	Avail and/or Special
A-1	

I. INTRODUCTION

The development of new approaches to electronic warfare require modern radar systems to use complex waveforms. These waveforms can be tested by using a copy of the transmitted pulse that has been stored for an interval corresponding to the round trip transit time to a target, and to which the expected Doppler frequency shift has been added. Programmable delays also allow true-time-delay steering techniques in phased-array radar to provide summation in the receive mode or distribution in the transmit mode that is independent of frequency. The very large delay-bandwidth product of fiber-optic devices make these types of devices superior for delay line applications compared to alternatives such as charge-coupled devices (CCDs), bulk wave devices, surface acoustic wave devices or digital RF memory systems. For example, losses at RF and microwave frequencies do not allow coaxial cables to provide long delay intervals. As frequencies increase, these losses increase and waveguides must be used in the millimeter frequency range. Surface acoustic wave delay lines are lossy, and the RF bandwidth is limited to approximately 1 GHz. Other high-frequency delay line approaches include magneto-static wave devices that make use of slow, dispersive spin waves in low-loss ferromagnetic materials and superconducting striplines operating at cryogenic temperatures. Digital RF memories (DRFMs) introduce spectral harmonics and have a limited dynamic range determined by the high-speed analog-to-digital conversion circuit. In addition, to circuit complexity and large power consumption, a digital RF memory has a much smaller bandwidth compared to fiber-optic delay lines.

Additional advantages of fiber-optic delay lines include the use of wavelength multiplexing to minimize the number of lines in a feed link, also the fiber is a nonconducting dielectric and does not disturb the RF field. Optical fiber is secure, EMI immune, and has mechanical flexibility, low mass, and small volume. Optical fiber has excellent transmission stability by virtue of the small ratio of the signal bandwidth to the carrier frequency. Moreover, the fiber approach does not require RF to digital, A/D or D/A converters, and it can support an information bandwidth of many GHz. For DRFMs the power consumption is determined by both the type and the length of the memory used. For large information bandwidth DRFMs use ECL or GaAs memory which leads to a typical system power consumption on the order of 100 W, more than that required for a large fiber-optic system.

For fiber-optic delay lines the attenuation along with the group velocity determine the maximum delay that can be achieved. If attenuation is high, then the delay must be kept relatively short, limiting the processing capabilities.

Loss and attenuation in a single mode fiber results from a number of wavelength dependent mechanisms including scattering, absorption, and externally induced losses such as those due to bending. For each of these mechanisms there exists certain wavelength ranges where their effect is minimal. However, the combined effect restricts the operation of fiber systems to a relative narrow spectral range from the visible to the near infrared.

Rayleigh scattering is the dominant loss mechanism in optical fiber below a wavelength of $1.55\text{ }\mu\text{m}$. As the electromagnetic wave propagates in the fiber, it is scattered by small (on the order of a few tenths of a micron) irregularities in the medium. This scattering process called Rayleigh scattering is strongly wavelength dependent. The attenuation per unit length is inversely proportional to the wavelength to the fourth power (*i.e.*, much lower at longer wavelengths than at short wavelengths.) For example, the loss per unit length at $\lambda = 0.83\text{ }\mu\text{m}$ is on the order of 3 dB/km whereas the loss per unit length at $\lambda = 1.3\text{ }\mu\text{m}$ is on the order of 0.5 dB/km (1 km corresponds to 5 μs delay).

At long wavelengths, infrared absorption losses (resulting from the vibration of the bonds between the glass constituents) limit the operation of most optical fiber systems to wavelengths of about $1.6\text{ }\mu\text{m}$ and below. These absorptive losses combined with Rayleigh scattering loss yield a composite loss profile with a minimum (approximately 0.2 dB/km) near $1.55\text{ }\mu\text{m}$.

The maximum bandwidth or transmission capability of a delay line processing system is ultimately limited by dispersion in the delay medium. In general dispersion arises from the group velocity in the medium varies with frequency so that a signal which is formed from a distribution of frequencies is distorted after propagation through a delay line.

When single mode fibers are used, there exists an operating wavelength where the first derivative of the group velocity with respect to wavelength vanishes. At this so called "zero-dispersion" wavelength the modulation bandwidth of the fiber is limited only by higher-order dispersion effects.

At wavelengths well-away from this zero-dispersion point the modulation bandwidth of a single mode fiber is dominated by first-order dispersion effects. At the wavelength of zero dispersion, higher-order dispersion effects set an upper limit on the modulation bandwidth.

Dispersion in silica-based fibers arises from the dispersive characteristics of the waveguide and the bulk material. If only material dispersion is considered, the zero dispersion wavelength occurs at $1.3\text{ }\mu\text{m}$. When waveguide effects are included, the minimum dispersion point is shifted. For most fiber constructions the shift is small, although in some cases as in so-called dispersion shifted-fibers the minimum dispersion is made to coincide with the wavelength of minimum loss ($\lambda = 1.55\text{ }\mu\text{m}$). In either case, when the operating wavelength coincides with the zero-dispersion wavelength, the modulation bandwidth is quite large. For example, a 150 km length of fiber (corresponding to a delay of 750 μs) has a bandwidth limited by dispersion of over 150 GHz.

In practice, however, these large bandwidths are difficult to realize because of polarization dispersion. Polarization dispersion arises from non-circular fiber cores and residual stress which cause the two polarization mode in a single-mode fiber to propagate at different velocities. Even still, if proper care is exercised in winding and handling, the dispersion of most commercially available fiber is approximately 0.1 ps/km. At lengths of 100 km this corresponds to frequencies of well over 20 GHz.

If even larger bandwidth is needed, polarization maintaining fibers can be used. At the largest lengths that we anticipate needing, polarization dispersion will not be a factor.

One possible type of fiber-optic delay is a recirculation delay line. The principal shortcoming of a fiber-optic recirculating delay line is the noise build-up, leading to faster deterioration in signal-to-noise ratio with increase in delay interval compared to that due to signal attenuation. Furthermore, the longest non-overlapping data stream is limited to the length of the recirculating loop. The duty cycle of the recirculation delay line is thus a function of the delay interval, and it is inversely proportional to the number of recirculations.

During the past, the development of programmable fiber-optic delay lines capable of long delay intervals has been hindered by a lack of fiber-optic switches with the desired characteristic of fast switching, low insertion loss and high isolation. Nanosecond switching time (available with electro-optic switches is thus a highly desirable feature). Electromechanical and thermo-optic switches are slow and thus can achieve only about a 1 ms switching time.

For example, the parameters of a programmable delay line for a radar moving target simulator are determined by the range of the radar to be tested, the desired range resolution, and the speed of the moving target. If the radar to be tested has a range of 50 nautical miles (93 km), the range corresponds to a round trip transit time of about $620 \mu\text{s}$. If the desired range resolution is 10 ft, the incremental delay interval would be 20 ns. With a propagation delay in the fiber of $5 \mu\text{s}/\text{km}$ ($5 \text{ ns}/\text{m}$), the required total fiber length of the delay line is about 130 km, programmable in 4 m increments. In other words, a 15-bit fiber-optic delay would meet the system requirements ($2^{15} = 32768$, and $32768 \times 20 \text{ ns} = 655.36 \mu\text{s}$; a slightly more accurate calculation is provided later). Even using the low-loss transmission window at 1550 nm where the fiber has a loss coefficient of about 0.2 dB/km, fiber attenuation would reach about 25 dB. Switches and splicing losses would add an additional 4 to 5 dB per switch ($15 \times 5 \text{ dB} = 75 \text{ dB}$). Thus the total loss could reach nearly 100 dB in a fiber-optic programmable delay line at maximum delay. For a required system dynamic range with 0 dB system gain, this loss problem must be solved. Fortunately, the loss problem can be solved with erbium-doped optical fiber amplifiers (EDFAs).

With our fiber-optic approach to a 15-bit programmable delay line, significant advantages can be achieved by using electro-optic (EO) modulators and switches. The EO modulator and switch approach offers extraordinary bandwidth (for nonlinear polymers, $>100 \text{ GHz}$), improved impedance mismatch compared to other methods, large dynamic range, and high sensitivity. There are other advantages of EO modulators and switches. For example, channel waveguides are compatible with optical fibers, allowing fibers rather than free space to transmit the optical signal. Because a fiber bundle is used, optical alignment between the source and switches and fiber amplifiers is more flexible and rugged than a free-space or mechanical approach.

In order to obtain the maximum possible bandwidth (> 16 GHz) and rapid switching time ($< 1 \mu\text{s}$), we will focus on recent developments in nonlinear optical polymer technology. It is well-known that organic polymers are already important materials in various electronic and photonic applications. Some examples are: packaging and interconnection of electronic components, coatings for optical fibers, optical recording media, polymeric waveguides and lenses, and microlithography.¹ Polymers also show prospects as active constituents of optical and electronic devices.² With these applications in mind, the important properties of polymers to be developed are physical phenomena like nonlinear optical response, dielectric constant, and electrical conductivity. In order to be really useful, the polymers should retain such properties as mechanical strength and ease of processing. With our novel approach combinations of properties will provide new classes of active materials for use in devices. For example, the nonlinear polymer in an electro-optic modulator or switch serves the dual functions as both a light-guiding channel as well as the nonlinear electro-optical medium. Other functions supporting velocity matching and device fabrication can also be incorporated.

As a result, the use of organic nonlinear materials is very attractive for external modulators and switches providing large bandwidth and short switching delay in the 15-bit programmable delay line. The materials can have a much larger electro-optic coefficient and smaller dielectric constant than lithium niobate. This allows a smaller drive power, with reduced weight and size, increased sensitivity, and an even larger frequency response because of a better velocity match between the optical and microwave signals. Moreover, the polymeric nature of the materials allows the use of different and less expensive fabrication techniques than does conventional lithium niobate with titanium diffused waveguides.

During Phase I our objective is to develop new, digitally-programmable, fiber-optic delay lines for wideband microwave signals. Our unique approach will use novel, polymeric switches and electro-optical modulators, together with a 1550 nm source, optical fiber amplifiers, and fiber delay lines. The use of nonlinear optical polymer switches and modulators provides not only very large bandwidth modulation but also fast switching time with low insertion loss and high isolation. The nonlinear optical polymers provide devices with large electro-optic coefficients, small dispersion, larger frequency response, and greater fabrication flexibility compared to LiNbO_3 or GaAs waveguide technology. Various types of polymer-based modulators and switches with optical fiber amplifiers have been considered in Phase I for applications to programmable fiber-optic delay line networks and device development in Phase II. The use of polymer materials will provide improved frequency response (potentially to 100 GHz), fast switching speed, larger electro-optic effect, lower cost, and greater manufacturing flexibility.

¹ F.A. Vollenbroek and E. J. Spiertz, "Polymers for high technology," ACS Symp. Series 346, American Chemical Society, Washington, D.C., 1988.

²A. F. Diaz, J. F. Robinson and H. B. Mark, Adv. Pol. Sci., 84, 113 (1988).

The technical objectives during Phase I were to explore and develop novel approaches for the applications of polymeric optoelectronic devices for wideband programmable microwave delay line applications. Specific technical goals for the programmable delay line include the following:

- Signal bandwidth > 16 GHz
- Optimum performance in the 9-11 and 3-5 GHz regions
- Signal dynamic range of 40 dB
- System gain 0 dB \pm 1.5 dB over signal bandwidth
- Delay variability 0 to 655.34 μ s, digitally programmable in 20 ns steps
- Delay switching speed < 1 μ s (200 ns desired)
- Minimum throughput delay < 100 ns
- Spurious products including triple transient response -35 dBc or less
- Operating temperature 0 to +50 °C
- Equalization for path and temperature variations
- Delay variation over operating range < 1 ns
- Architecture such that there is no loss of signal in the pipeline
- Reduced size, cost and power requirements compared to DRFM methods

II. RESULTS

Our approach to a programmable delay line is based on fiber-optics and very broadband EO modulators and switches to obtain the required signal bandwidth and very small switch delay as illustrated in Figure 1. This approach will allow a very low noise laser source (low RIN < -165 dB/Hz) such as a diode-pumped Er³⁺ laser or low-noise InGaAsP DFB laser at 1.55 μ m to be used with an external Mach-Zehnder modulator. This choice of wavelength provides the lowest attenuation thus limiting the number of fiber-optic amplifiers to ensure a 0-dB gain link with automatic gain control at the receiver with maximum delay. Our proposed architecture is based on a binary delay line formed by optically routing the signal through N fiber segments whose lengths successive increase by a power of 2. The required fiber segments are addressed using an array of N 2x2 optical switches. Each switch allows the signal to either connect or bypass a fiber segment a delay T may be inserted which can take any value in increments of ΔT up to a maximum value given by

$$T_{\max} = (2^0 + 2^1 + 2^2 + \dots + 2^{N-1}) \Delta T = (2^N - 1) \Delta T .$$

With N = 15 and $\Delta T = 20$ ns then T_{\max} is 655.34 μ s the required maximum delay. The delay interval can be achieved for ΔT with a fiber length of 4m. The fiber approach will also achieve the minimum throughput delay of 100 ns by use of only a very short distance between the source and receiver when

each of the 15 switches is in the bypass configuration. This can easily be much less than the required 100 ns duration. Thus this approach achieves the delay variability, with 20 ns programmable steps, and also achieves the minimum throughput delay.

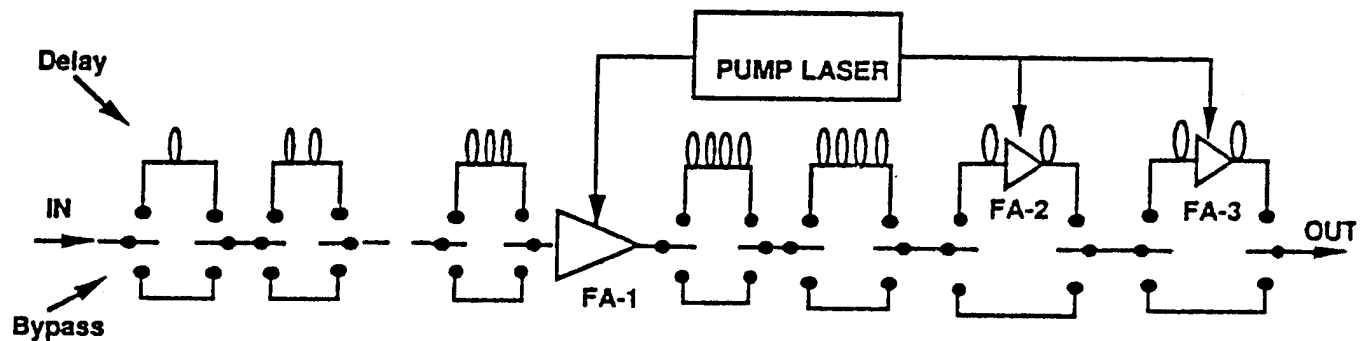


Figure 1. Schematic diagram of proposed programmable microwave fiber-optic delay line with nonlinear polymer electro-optical bypass switches and various optical fiber amplifiers (FA) to compensate for switch and fiber attenuation.
High speed photoreceiver with AGC and low noise source laser with broadband nonlinear polymer EO modulator not illustrated in this diagram.

In order to achieve a signal bandwidth of >16 GHz, we will use nonlinear optical polymer modulators. Fortunately, this same technology also allows us to fabricate switches that provide the desired time delay. We fully expect that switch delays of <100 ns can be achieved with proper switch design. Additional details are provided later in this report.

In determining the requirements for modulators and switches, several different device geometries have been discussed in the literature, and only a few will be considered here. For modulators, the common requirement is to induce electrically a phase shift $\Delta\phi$ in the optical fields of the order of π , as they pass through the electro-optic guiding region. The requirement on the electro-optic coefficient, r , may be estimated from

$$\Delta\phi = 2\pi/\Delta n/\lambda \approx \pi,$$

where l is the path length through the medium, Δn is the electrically-induced index of refraction change, and λ is the free space wavelength. The Pockels' coefficient, r_{eff} , is related to the induced index change by the relation

$$\Delta n = r_{\text{eff}} n^3 E/2,$$

where E is the applied electric field and n is the index of refraction.

For delay line applications the free space wavelengths are approximately 1310 nm or 1550 nm which are now in use for long range communications. In order to determine the required electro-optic coefficient we can use the previous two equations and assume a device length of 1 cm with modulating fields of approximately 1 V/ μm ; these assumptions require that $n^3 r_{\text{eff}} \approx 100 \text{ pm/V}$.

Nonlinear polymer devices can also be used for modulator applications to achieve the desired signal bandwidth of 16 GHz. For modulator applications there is no question that much greater bandwidths can be achieved. One scientist at TACAN has already demonstrated 60 GHz operation of electro-optic modulators based on nonlinear optical polymers. A question that we addressed in our Phase I investigation is the desired properties of state-of-the-art materials that would be available for a Phase II prototype system.

There are several issues relating to the desired properties of the electro-optic (E-O) polymer materials from different perspectives; these include the optical, electrical, mechanical and thermal properties. In fact, other properties such as chemical properties and the ease of device processing are also important.

The linear and nonlinear optical properties

E-O switches or modulators are nonlinear optical devices, therefore, the first requirement is a sufficient nonlinearity for device application. As mentioned previously, a practical measure of the nonlinearity for E-O applications (either switches or modulators) is $n^3 r$. In addition, the material must have excellent linear optical properties since the optical beam will travel a few centimeters in the waveguide. The index of refraction should have requirements to facilitate single mode waveguide

fabrication and fiber attachment. The index difference between the active waveguide and the cladding layers must satisfy the following relation for a single mode device

$$\Delta n \leq \lambda^2 / (8nd^2) \quad (1)$$

where λ is the wavelength of the optical beam, d is the thickness of the active waveguide region, and n is the index of refraction of the guiding layer. To match a single-mode 9- μm core-diameter commercial fiber, assume d is 5 μm , λ is 1.55 μm , then $\Delta n \leq 0.005$ is required for single-mode operation. The thickness of the cladding layers also should be on the order of 5 μm each, and therefore the total thickness will be in the near 15 μm . For most optical polymers, the index of refraction is in the range from 1.4 to 1.8. Also, any significant optical absorption will cause substantial optical power loss and lower the optical damage threshold. The power density in a waveguide is typically 10^5 to 10^6 W/cm². For PMMA based NLO polymers, the intrinsic loss due to C-H overtones is approximately 0.2 dB/cm. Many newly-developed fluorinated polymers show much lower intrinsic loss since the concentration of the C-H bonds is reduced as CH₃ groups are replaced by CF₃. The optical damage may also result from isomerization when the wavelength is close to the absorption band or from a slow photochemical reaction even the working wavelength is far from the absorption peak. We will address this issue in the chemical stability section.

Thermal stability

Among all the thermal stability issues, the stability of the NLO properties is of most importance. The thermal stability of the NLO property requires 1) the NLO chromophores to be stable and 2) the alignment of the NLO chromophores to be stable at the working temperature and all the temperatures involved in device processing. The modulator and switches used for this application, for example, requires the NLO material to hold its alignment at a working temperature about 50°C. From manufacturing considerations, the device may have to survive the packaging temperature (usually a few minutes excursion at 200~300°C) if the current semiconductor chip packaging process is used.

Chemical stability and processability

The material must be chemically stable when exposed to the atmosphere, water, chemicals used in photolithography, and solvents for subsequent layer deposition in a multi-layer structure. On the other hand, the material should be soluble in the desired solvent with controllable viscosity. The polymer solution should match the surface property of the substrate, provide good adhesion to the substrate and electrode materials, and form a smooth film by conventional film casting methods. The solvent should be easily removed from the film. The thickness should be controlled in the range from 1~10 μm . The surface morphology is very important since the scattering loss from the roughness of the waveguide walls and index fluctuation is often larger than the intrinsic absorption loss.

Another important issue is the photochemical stability of the NLO chromophores either doped or covalently attached to the polymer matrix. It has been shown in many cases that the NLO chromophores can be destroyed (bleached) by ultraviolet light or even short wavelength visible light illumination. Photochemical degradation of the optical waveguides also has been found at 1.3 μm wavelength in a DANS-based (dimethylaminonitrostilbene) thermoplastic NLO polymer in which the waveguide loss increased significantly after a few hours of continuous infrared light illumination. Oxidization was identified as one of the reactions during photo exposure for DANS chromophores. Although only a few studies address this problem, we believe that many photo-bleachable NLO polymers may suffer from photochemical degradation. A careful design of NLO chromophores can eliminate the photochemical degradation effects.

Electrical properties

The polymeric materials have very desirable electrical properties. The dielectric constant, dielectric strength and loss tangent meet our requirements for many of the polymers. The most important electrical property is the bulk resistivity which should be higher than or on the same order of those in the cladding layers. As a result, the poling voltage will be mostly across the NLO layer rather than across the cladding layer. The alignment efficiency depends on the field applied to the NLO film. In our previous work, we only encountered the resistivity problem during the poling process when the environmental temperature is raised. Sometimes the resistivity requirement can be met by choosing the cladding materials whose glass transition temperature is in the same order or lower than that of the NLO layer, and the resistivity of the cladding layer is smaller when heated above the glass transition temperature. Adding conductive dopants in the cladding layer is not recommended for high speed application because the microwave loss will increase significantly in the conductive polymer layer. Part of the modulation power will be dissipated as ohmic heat in the conductive dielectric layers.

The desired material properties are summarized in Table I. Here the desired properties for nonlinear optical polymers are compared with LiNbO_3 and GaAs, two other materials that can be used for nonlinear optical E-O modulators and switches.

Based on our investigation, the NLO polymers which satisfy all of the desired material's property requirements as summarized in Table I are not yet available. The principal shortcoming is the desired larger E-O coefficient. However, we plan to use either side-chain polyimide or crosslinkable polymers with an E-O coefficient $>15\text{-}20$ pm/V to fabricate modulators and switches for Phase II applications. The major difference is that either longer waveguides or larger drive voltages will be required compared to the 'desired' values in Table I for the E-O coefficient. The current candidates are: Sandoz side-chain polyimide, Dow Chemical thermoplastic TP series polymers, and thermally crosslinkable polymers such as DR19 doped polyurethane or the AdTech Systems Research, Inc. amino-sulfone material.

Table I Desired material properties for high speed E-O modulators and switches

	Desired in NLO polymer	in LiNbO ₃	in GaAs
n^3r	> 300 pm/V	320 pm/V	60 pm/V
r	> 80 pm/V	30 pm/V	1.6 pm/V
n	1.5~1.8	2.22	3.34
$n_e - n_o$	0.005~0.007	0.005	0.004
ϵ_r	3~4	28	12
Loss dB/cm	< 0.5	< 0.2	1
Long term stable temperature	> 125°C	stable	stable
Packaging temperature stability	> 250°C	stable	stable
Damage threshold at 1.3 μm	>10 MW/cm ²	0.1~1 MW/cm ²	1 MW/cm ²
Glass Transition temperature	>300°C		
Bulk resistivity	>10 ¹⁴ ~10 ¹⁶ /cm ²		
Dielectric strength	> 400 V/ μm		

Currently, we are fabricating Mach-Zehnder modulators as part of a separate program. The information that is gleaned for that development will help us to choose a definite material for our Phase II investigation. As a result, we do not see any difficulty in meeting the 0-50 degrees Celsius temperature range for the modulators and switches.

The nonlinear optical polymer that is used to achieve the 16 GHz frequency response will also be used for switches to achieve submicrosecond switching speeds.

Although the final switch design has not been completed, numerous features of the structure have already been determined. The expected layout will include a standard Y-branch architecture. With our proposed NLO polymer approach this device has the advantage of being fabricated with conventional IC manufacturing equipment. The substrate is expected to be silicon with a $1\text{ }\mu\text{m}$ thick aluminum ground plane above the silicon. Three polymer layers will include 1) a $3\text{--}5\text{ }\mu\text{m}$ -thick cladding layer, 2) a $2\text{--}5\text{ }\mu\text{m}$ -thick nonlinear polymer middle layer, and 3) a top cladding layer. After a metallic layer (*e.g.*, gold) is placed above the top cladding layer the polymer can be poled in an electric field of approximately $50\text{--}100\text{ V}/\mu\text{m}$ at the glass transition temperature. The top metallic layer is subsequently patterned to allow the waveguide formation and the fabrication of a top microstrip electrode above the waveguide.

The waveguides can be formed by reactive ion etching in the middle polymer layer with an IC mask aligner and a gold microstrip electrode formed above the top cladding layer. With an index change of 0.005 below that of the channel, single mode operation is possible, and the waveguide may be efficiently coupled to an optical fiber. The approximate expected microstrip cross sectional size is $10\text{ }\mu\text{m}$ by $20\text{ }\mu\text{m}$ with a 15 mm electrode length.

In order to couple optical waveguides in polymer films to external devices, it is desirable to first couple the waveguides to optical fibers. Endfaces can be made on the substrate by cleaving the silicon substrate. The fiber-to-waveguide coupling loss can be estimated from the fiber diameter and the waveguide cross-sectional dimensions. This loss is expected to be approximately 0.75 dB per facet. For this work, we are concerned with single-mode waveguides, so the alignment tolerances involved are typically about $0.2\text{--}0.5\text{ }\mu\text{m}$. In order to achieve this type of precision, we expect to prepare alignment features on the same substrate which supports the polymer waveguide structure. These alignment features will determine the position of the optical fibers which will be coupled to the polymer film. We are currently perfecting this fiber-to-waveguide attachment under another program.

The alignment features can be formed by a number of techniques. The best established technique uses V-grooves etched into the substrate. The sides of the V-groove provide both horizontal and vertical alignment for the fiber. Our interest is in the use of thick ($>60\text{ }\mu\text{m}$) polymer films to form alignment features that provide horizontal alignment of the fibers. The vertical alignment of the fibers is provided by the exposed surface of the substrate.

We have previous experience with this approach, but its application was limited by the quality of the polymer used. The problems which we experienced were related to the environmental instability of the polymer as the temperature was varied. This instability resulted in movements of the fiber which were several micrometers in size. As a result, we are now using channels produced directly in the silicon or ceramic substrates for all of our commercial efforts—even though this requires extra fabrication steps.

The requirement of large frequency response dictates materials with low dielectric constants to minimize device capacitance for a lumped device. To improve the high-speed operation in guided wave electro-optic devices a traveling-wave electrode can be employed in which the optical and the RF wave travel codirectionally at similar speeds, thus extending the frequency response limits due to electronic transit time. Here the electrodes are chosen to have an impedance match to the input signal transmission line. The velocity mismatch between the optical and the RF waves is proportional to the difference between the effective wave vectors. For example, in LiNbO_3 the difference between the optical index of refraction and the square root of the dielectric constant is close to 2, yielding a mismatch limited bandwidth (electrical)-length product of approximately 6 GHz-cm. Although the bandwidth under velocity mismatched conditions can be improved with special electrode waveguide structure designs, this is typically associated with low modulation efficiency or phase distortion. Organic nonlinear materials, by contrast, are ideally suited for high-speed modulation by virtue of their low dielectric constant and the excellent match between the RF and the optical propagation velocities. With these materials, bandwidth-length products exceeding 100 GHz-cm are expected.

The current best performances reported in major scientific publications for the electro-optic polymer modulators are summarized as following:

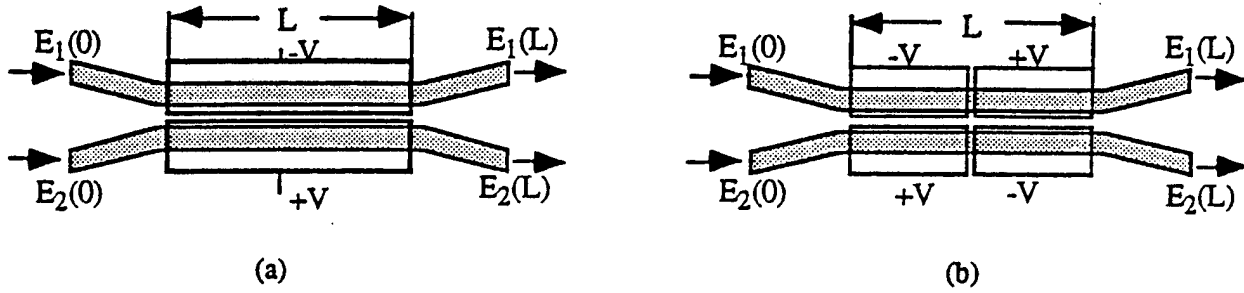
half-wave voltage V_p :	5 - 10 V
insertion loss:	~6 dB
thermal stability:	200 °C
frequency response:	60 GHz
extinction ratio I_{\max}/I_{\min} :	>20 dB

There are also new improvements in the synthesis of electro-optic polymer materials. Electro-optic coefficients in the range of 40 to 50 pm/V have been reported by different groups. Using these materials, one can further reduce the required RF driving power and the size of the modulators. It is possible to fabricate ultrawide bandwidth polymer modulators with RF driving power only a fraction of that required by a similar lithium niobate device with these new materials. The optical insertion loss can be further reduced by a better matching of the waveguide and cladding materials or by using a tapered fiber to waveguide transition section. We expect insertion losses of 3-4 dB with a minor change in our pigtailling method. These research projects are currently under intensive study at TACAN and other organizations. Also we are currently exploring ways of further reducing the insertion loss in the switches.

Because the switches will be fabricated by techniques very similar to the modulator (a different mask will be used), these results give us great confidence in our ability to produce the necessary switches for the switching elements.

Directional coupler switches consist of two side-by-side waveguides separated by only a few microns,

as shown in Figure 2. The overlap of the guided wave in the two wave guides couples energy back and forth between the waveguides. When the switching voltage is applied to an electro-optic directional coupler, the power exchange can be controlled by either phase difference or coupling coefficient changes induced by the applied field. However, the modulation of phase difference is more effective than the coupling coefficient change in couplers made from electro-optic materials.



Figures 2. Schematic structure of (a) a conventional directional coupler and (b) a $\Delta\beta$ -reversal electro-optic directional coupler.

A directional coupler switch is a four-terminal device that allows two inputs and two outputs. The information from the optical beams can be exchanged between two waveguides. The output fields of the two output terminals are related to the two inputs by the solution of the coupled wave equation. A conventional electro-optic directional coupler switch consists of a coupled waveguide section in electro-optic materials and a set of electrodes. The applied electric field at a specific time is unidirectional, that is, only one field direction is available at a time. In this arrangement, if the input optical fields are $E_1(0)$ and $E_2(0)$, the two output optical fields of the coupler are

$$E_1(L) = E_1(0) \left(\cos \beta_0 L + j \frac{\Delta\beta}{2\beta_0} \sin \beta_0 L \right) + E_2(0) \frac{\kappa_{12}}{\beta_0} \sin \beta_0 L$$

$$E_2(L) = E_1(0) \frac{\kappa_{21}}{\beta_0} \sin \beta_0 L + E_2(0) \left(\cos \beta_0 L - j \frac{\Delta\beta}{2\beta_0} \sin \beta_0 L \right)$$

$$\beta_0 = \sqrt{|\kappa_{12}|^2 + \left(\frac{\Delta\beta}{2}\right)^2}$$

where κ is the coupling coefficient, $\Delta\beta$ is the phase mismatch between two waveguides, and L is the coupling length. It is easy to find that it is impossible to obtain complete power exchange between two channels when $\Delta\beta \neq 0$. The extinction ratio is not adequate for applications where high dynamic range is required. For high dynamic range applications, we will use the so-called $\Delta\beta$ -reversal method to obtain high extinction ratio. A $\Delta\beta$ -reversal coupler has two or more sets of electrodes. Electric fields are applied with alternating directions among electrodes. The output of a two-section $\Delta\beta$ -reversal directional coupler can be expressed as

$$E_2(L) = E_1(0) \left\{ \cos^2 \frac{\beta_0 L}{2} + \left[\left(\frac{\Delta\beta}{2\beta_0} \right)^2 - \left(\frac{\kappa}{\beta_0} \right)^2 \right] \sin^2 \frac{\beta_0 L}{2} \right\} + E_2(0) \frac{2\kappa_{12}}{\beta_0} \sin \frac{\beta_0 L}{2} \left(\cos \frac{\beta_0 L}{2} - j \frac{\Delta\beta}{2\beta_0} \sin \frac{\beta_0 L}{2} \right)$$

$$E_2(L) = E_1(0) \frac{2\kappa_{21}}{\beta_0} \sin \frac{\beta_0 L}{2} \left(\cos \frac{\beta_0 L}{2} + j \frac{\Delta\beta}{2\beta_0} \sin \frac{\beta_0 L}{2} \right) + E_2(0) \left\{ \cos^2 \frac{\beta_0 L}{2} + \left[\left(\frac{\Delta\beta}{2\beta_0} \right)^2 - \left(\frac{\kappa}{\beta_0} \right)^2 \right] \sin^2 \frac{\beta_0 L}{2} \right\}$$

The complete power crossover occurs when

$$\sin^2(\beta_0 L/2) = \beta_0^2 / (2\kappa^2)$$

and the bar state (no power exchange) occurs when

$$\begin{aligned} \beta_0 L &= 2m\pi & \text{for all } \Delta\beta \\ \beta_0 L &= (2m+1)\pi & \text{for } \Delta\beta = 0 \end{aligned}$$

In a symmetric waveguide design, the initial phase mismatch is zero. One can adjust the coupling length or coupling coefficient to bias the device in either the crossover state or the bar state. However, for the best switching efficiency we want to adjust the product $\kappa L = \pi$ so that the switch is initially at the bar state. This arrangement results in the minimum phase change required for switching to the crossover state

$$\Delta\beta \approx 1.6\pi/L,$$

which corresponding to an index change of

$$\Delta n = 0.8\lambda/L.$$

The required index change is slightly smaller than a conventional directional coupler device in which $\Delta n = 0.866\lambda/L$. The advantage of the $\Delta\beta$ -reversal switch is the high extinction ratio. Complete switching can be obtained by controlling the applied voltage to the electrodes. Extinction ratios of 25-28 dB have been reported for LiNbO₃ devices. We expect similar, if not better results with nonlinear optical polymer waveguides.

The extinction ratio of the $\Delta\beta$ -reversal directional coupler switches depends on several factors, 1) scattering of the waveguides, 2) precise control of the applied voltages, 3) environment condition (such as temperature) fluctuation, 4) bandwidth of the optical signals, and 5) modal properties of the guided optical waves.

The scattering problem is essentially an issue of the waveguide quality. The waveguide must be smooth and uniform with minimum birefringence. The radiation loss at the waveguide transition period must be minimized. We can select NLO polymers with superior optical quality, and design an optimized photo mask in defining waveguides to overcome the scattering problem.

Control of the appropriate switch voltage plays an important role in high performance systems. We plan to use a reference source and synchronized detection system to control the switch voltage. The principle of this design is that we purposely modulate the input signal with a frequency outside the data bandwidth in one channel, then at the output side we split a small portion of the signals to a detector and monitor this frequency in both channels and minimize this signal in one channel by switch voltage control. Similar to a lock-in amplifier, high sensitivity and signal-to noise ratio can be obtained in this controlling system. We have successfully used this method in DC bias control circuits for electro-optic modulators. This active feed back system can also be used to compensate the changes due to environment temperature fluctuation and the drifting of the NLO property of the electro-optic polymer layers.

The detailed layout of the switching electrode depends on the required speed of the switching operation. For programmable delay line switching, the on and off speed can be in the order of microseconds to nanoseconds. A lumped circuit electrode design will be adequate. When the switching is designed for playing bit-by-bit, as those in optical computing, the switching speed must be high, and traveling wave electrodes should be used. With all of the switches in the bypass state, a total length of connected fiber, 20 m will give <100 ns delay, if < 4 m then the delay will be < 20 ns.

The extinction ratio can be affected by the dispersion of the waveguide, coupling coefficient. From the last equation given above, we know that the required index change for a crossover state, and therefore, the switching voltages are wavelength dependent. However, when the bandwidth is narrow, the effect of these coupling dispersions is negligible. An important factor to note about the switches is that a 25-30 dB optical switch isolation corresponds to a electrical isolation of 50-60 dB.

During Phase I we explored the use of optical amplifiers to ensure that the system gain can be maintained at 0 dB over the entire signal bandwidth for various programmable delays. The use of optical amplifiers can boost the signal that is lost by traversing the fiber delay lines. The system gain can be maintained at 0 dB by the use of a combination of optical amplifiers and electronic amplifiers at the receiver. Equalization circuits at the receiver can compensate for the frequency dependence of the link gain. This frequency dependence is, however, expected to be small. TACAN has historically used this approach in previous work to maintain a constant link gain over a specified frequency range. In addition, other effects such as temperature changes in link performance can also have compensation circuits at the receiver. With this approach, the input signal can be amplified to drive the modulator with the necessary voltages. During this report we will also examine the dynamic range of the system. Spurious products can be reduced to provide a maximum dynamic range by a combination of 1) maintaining the Mach Zehnder modulator at its proper bias point, thus eliminating all even-order distortions, and 2) a broadband predistortion circuit to maintain the third and fifth order distortions at a minimum. The predistortion circuit produces the inverse distortion of the modulator around its bias point, thus giving a highly linear response to input signals.

In order to ensure that the transmitter is providing minimum distortions, a bias feedback circuit will be developed that will maintain the modulator at the quadrature point. This will keep the second-order distortions minimized. In general, we expect that temperature changes and stresses may cause the bias point to drift from the quadrature point. Using a fiber-optic coupler to sample a portion of the output signal, the harmonic of an injected pilot tone can be detected with a photodetector. The pilot tone is modulated by the Mach-Zehnder modulator, and if the modulator is not biased at the quadrature point, a tone at twice the frequency will be generated. A coherent feedback loop to control the modulator bias will be developed and can ensure that the modulator is maintained at the quadrature point to suppress all even-order harmonics.

In order to ensure that the system has a linear response with wide dynamic range, a linear receiver must be used. Our approach is to use an InGaAs Schottky photodiode. This type of photodetector has a very low dark current, fast response time and small capacitance. For example, InGaAs/InP photodiodes with responsivity in excess of 0.6 A/W at 1550 nm wavelength, and a bandwidth of 25 GHz are available commercially. These devices are already pigtailed to an optical fiber and mate to an SMA compatible connector. The receiver with equalization circuits will have a flat frequency response and a 50 ohm output impedance over the desired range of frequencies.

In evaluating fiber-optic system performance, the system dynamic range is measured from transmitter RF/microwave input to the output of the receiver. Dynamic range is defined as the ratio of the maximum receiver signal, limited by a level of acceptable distortions, compared to the minimum detectable receiver signal level, limited by system noise.

For the case with distortion created by a maximum allowable input signal $P_{s,max}$, the generalized

dynamic range is given by

$$DR = \frac{P_{s,maxi}}{N_f}$$

where

$$N_f = k \cdot T \cdot B \cdot NR$$

is the system noise floor. If typical amplifiers are used in the system and the third-order intercept point is known at the amplifier input, P_{IP} , then

$$DR = \frac{P_{s,maxi}^3 / P_{IP}^2}{N_f}$$

The lower limit is for an input signal equal to the noise floor (referred to as the minimum detectable signal), and the upper limit is for an input signal just strong enough to produce third-order distortion products that are at the noise floor level. It can be shown that the nonlinearity of typical electronic amplifiers result in spurious-free dynamic range given by

$$SFDR = \frac{P_{s,iSF}}{N_f} = \left(\frac{P_{IP}}{N_f} \right)^{2/3}$$

Also, for comparative purposes the bandwidth can be left out of the noise floor calculation for typical electronic amplifiers retaining only kT and NF for a receiver noise density N_{rx0} yielding

$$SFDR_0 = 10 \log \left[\frac{P_{IP}}{N_{rx0}} \right]^{2/3} \quad \text{dB} \cdot \text{Hz}^{2/3}$$

A high sensitivity photodetector diode remains reverse biased throughout the information cycle. In practice, the distortion produced by InGaAsP photodiodes is below link noise levels when the optical input power remains less than 1 - 2 dBm. To the extent that a Mach-Zehnder can be perfectly linearized, the unamplified link behaves ideally linear and a theoretical dynamic range can be calculated based on the limitations of (1) maximum signal power from the photodiode, and (2) total noise power density at the photodiode output.

Neglecting optical amplifier noise, the RF/microwave modulation signal-to-noise power ratio at the optical receiver can be found from

$$S/N = \frac{0.5(M \cdot \Re \cdot P_r)^2}{rin \cdot B \cdot (\Re \cdot P_r)^2 + 2 \cdot e \cdot B \cdot \Re \cdot P_r + 4 \cdot k \cdot T \cdot NR \cdot B / TZ}$$

where $rin = 10 \cdot \log^{-1} RIN$ and

\mathcal{R} = photodetector responsivity, A/W

P_r = received optical power, W

B = RF bandwidth, Hz

e = electron charge, Coulombs

m = RMS modulation index

RIN = laser relative intensity noise (dB/Hz)

k = Boltzmann's constant, 1.3×10^{-23} W/K·Hz

T = receiver temperature in Kelvin, K

NR = receiver noise ratio (NF)

TZ = receiver transimpedance in Ω

The terms in the denominator are noise power (amperes squared) contributions from the laser (RIN), photodiode shot (\propto average diode current), and kTB noise of the post detector electronics including any transimpedance amplifier (gain = TZ), if used. Years of experience with high quality photoreceivers at TACAN allows us to replace the last term with an equivalent noise current density for the post detection electronics of less than or equal to 49×10^{-24} A²/Hz ($i_{na} = 7$ pA/ $\sqrt{\text{Hz}}$). If we assume a received optical power of 1 mW, we can calculate the various noise terms.

1. laser RIN ≤ -160 dB/Hz: $rin(\mathcal{R}P_r)^2 = 10^{-16} \cdot (0.8 \cdot 10^{-3} \text{ A})^2 = 0.64 \times 10^{-22}$ A²/Hz
2. Shot noise: $2 \cdot e \cdot \mathcal{R} \cdot P_r = 2 \cdot 1.6 \times 10^{-19} \cdot 0.8 \cdot 10^{-3} = 2.56 \times 10^{-22}$ A²/Hz
3. kTB equivalent noise: $7 \text{ pA}/\sqrt{\text{Hz}} \rightarrow i_{na}^2 = 49 \times 10^{-24}$ A²/Hz

Total noise power density is the sum: $i_s^2 = (0.64 + 2.56 + 0.49) \times 10^{-22} = 3.7 \times 10^{-22}$ A²/Hz. Thus for sufficiently intense optical signal shot noise-limited detection can be maintained.

The addition of optical amplifiers in the signal path will add other noise terms due to amplified spontaneous emission from the amplifier. Multiple noise terms are possible that include signal-spontaneous emission interactions with itself and with signal wavelength.

In typical performance testing, receiver signal is the result of modulating two tones (two, unequal frequency, RF/microwave sinusoids) on an ideally linear MZI modulator. Each tone is modulated to $m = 0.5$ in order that the peak modulation envelope does not exceed 100 percent, but maximum possible SNR is measured over the link. Hence, the receiver signal power is calculated as

$$\text{Signal (2-tones at } m = 0.5 \text{ per tone)} = 0.5 \cdot (0.5)^2 \cdot (0.8 \text{ A/W} \cdot 1 \times 10^{-3} \text{ A})^2 = \underline{80 \times 10^{-9} \text{ A}^2}.$$

Combining the resulting signal and noise results in the S/N equation above, yields the per-tone SNR:

$$\frac{S}{N} = \frac{80 \times 10^{-9} \text{ A}^2}{3.69 \times 10^{-22} \text{ A}^2/\text{Hz}} = 21.68 \times 10^{13} \text{ (Hz)} = 143 \text{ dB} \cdot \text{Hz}$$

where Hz is not raised to the 2/3 power because the calculation is for maximum practical signal and noise, and not a projection based on a "well behaved" nonlinear system using a theoretical third-order

intercept (TOI). It is to be recognized that any amplifiers used as a transmitter pre-amplifier or for receiver post-detection amplification must have TOI's greatly exceeding their respective output signals. This simple calculation, however, illustrates that very large dynamic range links can be achieved. In addition, because the third-order is determined by the transmitter and receiver linearity, we will examine these with optical amplifiers in the optical circuits.

For a maximum delay of $655 \mu\text{s}$, the attenuation at 1550 nm corresponds to approximately 0.2 dB/km and the propagation delay is $5 \mu\text{s/km}$, thus the maximum fiber length is 131 km and the corresponding attenuation is approximately 26 dB. Additional losses occur at each switch and splice which are estimated to be approximately 5 dB per switch which is not due to the intrinsic loss in the switch, but rather to the loss at the fiber pigtailed to the switch. A total of 15 switches will be required to achieve the maximum delay. Thus the total switch loss can achieve 75 dB.

With erbium doped fiber amplifiers (EDFAs) gains of 15-20 dB are typical, and the gain can be changed by changing the input pump power to the amplifier. Thus for each 15 dB of loss, due to a combination of switch excess loss and fiber attenuation, the optical signal can be increased by 15 dB by an EDFA. Since a maximum of 100 dB loss is expected 6 EDFAs may be needed to compensate for the switch and fiber losses. The positions of the EDFAs in relation to the 15 switches will be discussed later in this report.

During Phase I we did experiments with erbium doped fiber amplifiers (EDFAs) on RF modulated signals. Here our interest was in the determination of how the EDFAs can be used to compensate for the switch and fiber losses. For example, we have measured the performance of an EDFA link in order to confirm that we can achieve large signal-to-noise ratio as well as small second- and third-order distortion products with an EDFA system. Here our initial experiments were limited to a single EDFA, although other researchers have very recently demonstrated that three cascaded EDFAs can provide a 50-dB power budget with third-order distortion less than -55 dBc.³

With our experimental approach a 980 nm pump laser is used to achieve a low noise amplifier. The use of 980 nm EDFA pump simplifies optical filtering of the pump source compared to a 1480 nm pump.

Figures 3 and 4 illustrate our experimental apparatus without and with the EDFA.

Here we used a 1550 nm DFB laser as a source, a Mach Zehnder modulator as an optical modulator, a custom EDFA, a Hewlett Packard HP70904A spectrum analyzer, an IPITEK photoreceiver, and

³ W. Muys, J.C. van der Platts, F.W. Willems, H.J. van Dijk, J.S. Leong, and A.M.J. Koonen, IEEE Photonics Tech Lett. 7, 691 (1995)

a Matrix Multicarrier generator with an 80 channel output. The optical gain of the EDFA was determined by the input signal and was determined as: 19 dB at -3 dBm input, 24 dB at -10 dBm

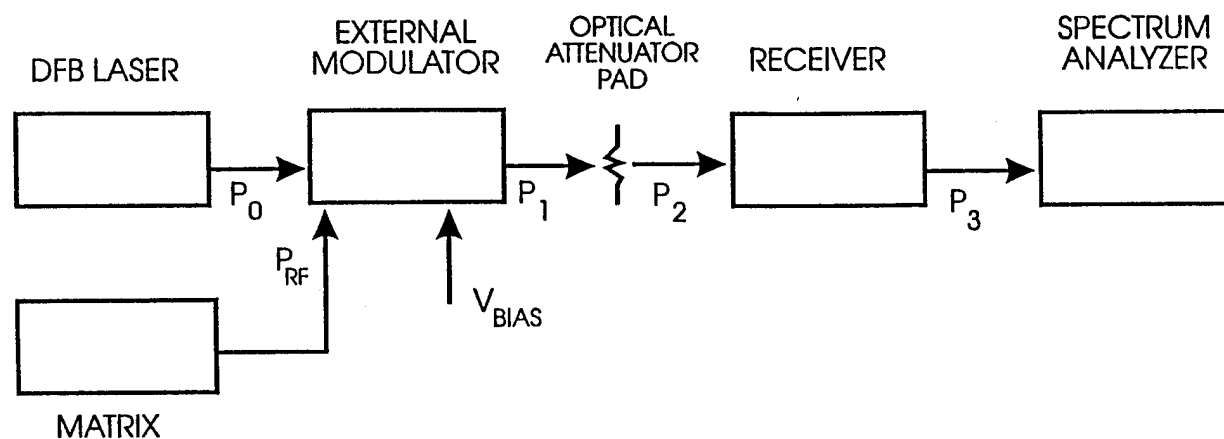


Figure 3. Schematic diagram of test set-up without EDFA

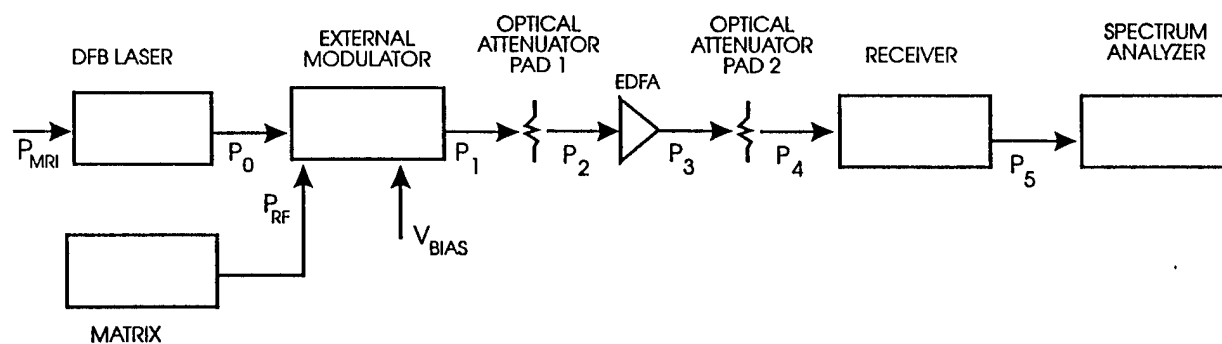


Figure 4. Schematic diagram of test set-up with EDFA

input, and 31 at -20 dBm input.

In order to determine the effect of the EDFA on carrier-to-noise ratio (CNR), second-order distortions (CSO) and third-order distortions (CTB) several experiments were conducted. First, the CNR, CSO, and CTB were measured as in Figure 3 without and EDFA. Next, these same figures of merit were measured with an EDFA as illustrated in Figure 4. Table II shows a comparison of these results. Here data were obtained with 0 dBm power on the receiver in both cases, with 10 dBm for the output power of the laser. Data were obtained at three different carrier frequencies: 55 MHz, 331 MHz, and 547 MHz.

The data show that carrier-to-noise ratios of greater than 46 dB can be achieved. The lower CNR after the EDFA compared to the system without an EDFA is a result of the relatively large noise figure for our EDFA. Also the CTB is greater than 63 dBc, much lower than the target of 35 dBc. Here the differences between the CTB with and without the EDFA are thought to be due to the limitations in our measuring technique. Also the authors of Reference 3 cited above also observed CTB as approximately -55 to -65 dBc and independent of network layout and number of EDFAs. The CTBs are thus determined by how linear the modulation scheme is.

TABLE I

A.	No EDFA	55 MHz	331 MHz	547 MHz
	CNR	52	53	51
	CSO	62	65	65
	CTB	59	61	56
B.	With EDFA			
	CNR	46	46	48
	CSO	59	65	66
	CTB	65	65	63

Based on the expected switch loss (assumed to be 5 dB) per switch and the fiber loss, we have determined the following as the initial design for the binary delay line. Amplifiers will be positioned at the following locations: 1) before S1, 2) after S3, 3) after S6, 4) after S9, 5) after S13, and 6) after S15. Note, that the first EDFA is placed after the NLO polymer modulator and before the first switch. If the switch loss can be reduced significantly below the assumed 5 dB, then the number of EDFAs can be reduced.

Also during Phase I we have performed numerous mathematical simulations on the expected effect of the EDFA on the signal-to-noise ratio. These simulations were done with 3 EDFA in the link. The results show that with an assumption of reasonable noise in the EDFA, a dynamic range of greater than 40 dB can be achieved. These calculations and software will be provided separately to the government.

During Phase I the effect of temperature on the delay was investigated. Here the change in the delay δt_d is given by

$$\delta t_d = (n \delta L + L \delta n)/c$$

where L is the length of the fiber, c is the vacuum speed of light, and n is the index of refraction of the fiber.

If we assume that L is the maximum possible length, corresponding to the maximum delay, then $L = 131$ km.

The change in delay can be rewritten as

$$\delta t_d = L [(dn/dT) \Delta T + n\alpha \Delta T]/c$$

where α is the coefficient of thermal expansion and ΔT is the temperature change.

Using data from Corning for standard single mode fiber, we have $\alpha = 0.5 \times 10^{-6}/^\circ\text{C}$ and $(dn/dT) \approx 6 \times 10^{-6}/^\circ\text{C}$. If the maximum temperature change is 25°C corresponding to a 25°C change from a starting point of 25°C , then the maximum time delay is expected to change by approximately 72 ns, or approximately 3 ns/ $^\circ\text{C}$.

There are several possible ways to compensate for this change. One method is to find a fiber that has a much smaller change in the delay with temperature. Recently, we have determined that such fibers exist with delays of an estimated 0.01 ppm/ $^\circ\text{C}$ from 10 to 20°C . For a maximum delay of 655 μs , this corresponds to 6.5 ps/ $^\circ\text{C}$ between 10 and 20°C . Currently we are examining additional properties of this fiber including its cost and availability for a Phase II program.

An alternate approach to compensate for the change in delay with temperature is to measure the delays at different switch settings at a well-defined temperature and to then adjust the switch settings at the least significant bit level to compensate for the temperature effects. Thus, to maintain a specific delay over the temperature range from 0 to 50°C , the switches at the least significant bit level would be adjusted to conform to the desired delay to within 20 ns, the delay of the shortest delay-line interval. This approach would require a temperature calibration of the programmable delay and a

thermometer to measure the temperature in the cavity that would house the various spools of standard single-mode fiber. Once the temperature is determined, a computer program would calculate the effect on the delay with the current switch settings and then reset one or more switches to readjust the delay. For example, a 5 degree increase in temperature would cause an increase in delay of approximately 15 ns with standard single-mode fiber when the delay line is set for maximum delay. Then the switches could be reset to decrease the delay by 20 ns (the least significant digit). This would place the delay within 5 ns of the desired delay. A simple 486 or 586 microprocessor with associated memory could easily provide this calculation.

A third method is simply to determine the actual delays and subsequently correct the data in order to compare it to a standard temperature state.

A fourth method is to maintain the fiber in a temperature-regulated environment with the temperature stabilized to within 0.3°C.

One possible application of the programmable delay is in a ranging simulator. Here, there was some concern that data could be lost as the delay-line was switching from one state to another. We have examined this potential problem and have determined that for decreasing range, no data will be lost.

To understand this effect we have considered a 5-bit switching delay line. For a 15-bit device the principle is the same. For the 5-bit device, consider a simulation at the maximum range. This would correspond to a set of switches with the maximum delay - call this switch array state {11111}. The next shortest time delay would be state {11110}, and the next shortest state {11101}. Here the binary digit at the far left is the most significant state switch and the binary digit at the far right is the least significant state switch. For a device traveling at 300 m/s, a 2 m minimum range resolution (corresponding to 20 ns round trip delay in an optical fiber) would correspond to 6.6 ms time between successive switches. Note, that from state {11111} to state {11110}, there is no change in switches except the least significant bit. Thus light traversing the last four switches would not change its path from one state to the next. Even for transitions from states such as {11000} to state {10111} there is no lost signal. Here light bypasses the first three delays and traverses the last two delays for state {11000}. For the next state, the signal will propagate through the first three delays, bypass the fourth delay and traverse the last delay. In the switching from one state to the other, any signal left in the last two delay lengths will continue to propagate to the detector because the last switch does not change states. The next to last switch changes, but it is *before* the last two delay lengths.

We have examined all 32 possible conditions for a 5-bit switch from the {11111} to the {00000} state. In the transition for the any one state to the next state of less delay, no signal will ever be trapped in the delay line. Trapping becomes a problem if one switches between states that do not differ by a least significant bit, for example, from a state such as {11101} to a state {00011}, but this is not the type of state switching that would be encountered in a ranging application.

Another method of ensuring that no data are lost is to use a dual delay line. Here, a control processor will switch from delay line to the second for sequential switch settings. This dual delay line approach ensures that any data in one line will always be emptied as the second delay line is used. The only requirement is that the switch from one delay to the other is at a speed of $<1\mu\text{s}$. With this approach the individual switches in the delay line can be somewhat slower, although the modulator must still respond to the 16 GHz goal.

We have also started to look at automatic gain control for ensuring that the gain can be fixed as the switches change. Here, the best way to achieve this is with a pilot tone at a low frequency, outside the band of any signals. The optical amplifiers and receiver gain would be adjusted to maintain a constant gain independent of switch states. Additional details will be provided in the Phase II proposal.

III. CONCLUSIONS

During this Phase I program we have examined how to use nonlinear optical polymer modulators and switches to develop a binary delay line. All of the desired properties can be achieved with a 15-switch delay line approach. The most challenging goal will be to reduce the delay variation with respect to temperature. We have determined four different methods of reducing the temperature effect of the delay.

IV. FUTURE

The next step is to fabricate a prototype binary delay line and test it in laboratory and under field operating conditions.